Supplementary Materials

Development of a Flexible and Conductive Heating Membrane via BSA-assisted Electroless Plating on Electrospun PVDF-HFP Nanofibers

Mun Jeong Choi[1,†], Dae Hyeob Yoon[2,†], Yoo Sei Park[3,4], Hyoryung Nam[5,*], Geon Hwee Kim[1,2,*]

1 Department of Mechanical Engineering, Chungbuk National University (CBNU), 1, Chungdae-ro, Seowon-gu, Cheongju-si, Chungcheongbuk-do, 28644, Republic of Korea; cmjanswjd@naver.com; geonhwee.kim@chungbuk.ac.kr

2 School of Mechanical Engineering, Chungbuk National University (CBNU), 1 Chungdae-ro, Seowon-gu, Cheongju-si, Chungcheongbuk-do, 28644, Republic of Korea; paul9453@naver.com; geonhwee.kim@chungbuk.ac.kr

3 Department of Nanoenergy Engineering, Pusan National University, Busandaehak-ro 63 beon-gil 2, Geumjeong-gu, Busan, 46241, Republic of Korea; yoosei@pusan.ac.kr

4 Department of Nano Fusion Technology, Pusan National University, Busandaehak-ro 63 beon-gil 2, Geumjeong-gu, Busan, 46241, Republic of Korea; yoosei@pusan.ac.kr

5 Department of Biomedical Engineering, Daegu Catholic University School of Medicine, 33 Duryugongwon-ro 17-gil, Nam-gu, Daegu, 42472, Republic of Korea; ryung@cu.ac.kr

† These authors contributed equally to this work.

* Co-correspondence: geonhwee.kim@chungbuk.ac.kr (Geon Hwee Kim); ryung@cu.ac.kr (Hyoryung Nam)

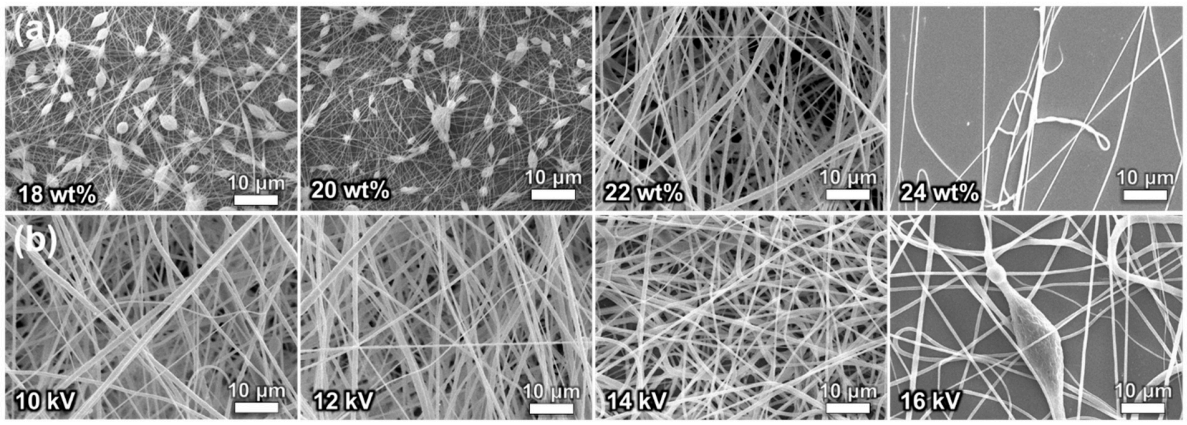


Figure S1. Morphological analysis of electrospun fibers under varying conditions. (a) SEM images of electrospun fibers with different polymer concentrations in the spinning solution (18, 20, 22, and 24 wt%). (b) SEM images of electrospun fibers fabricated under different applied voltages during electrospinning (10, 12, 14, and 16 kV).

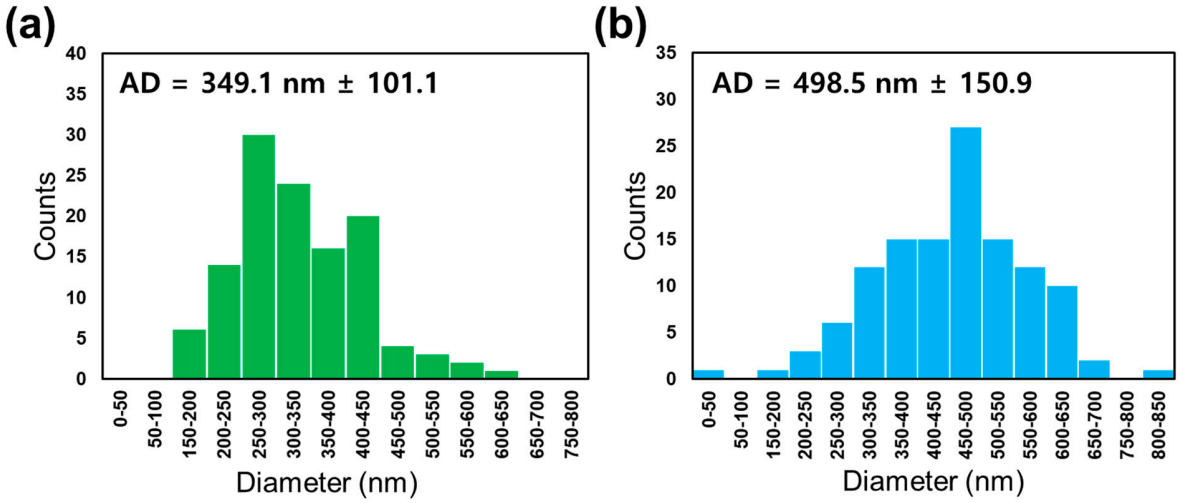


Figure S2. Diameter distribution of electrospun nanofibers. (a) Frequency histogram of nanofiber diameters immediately after electrospinning. (b) Frequency histogram of nanofiber diameters after immersion in SDBS solution.

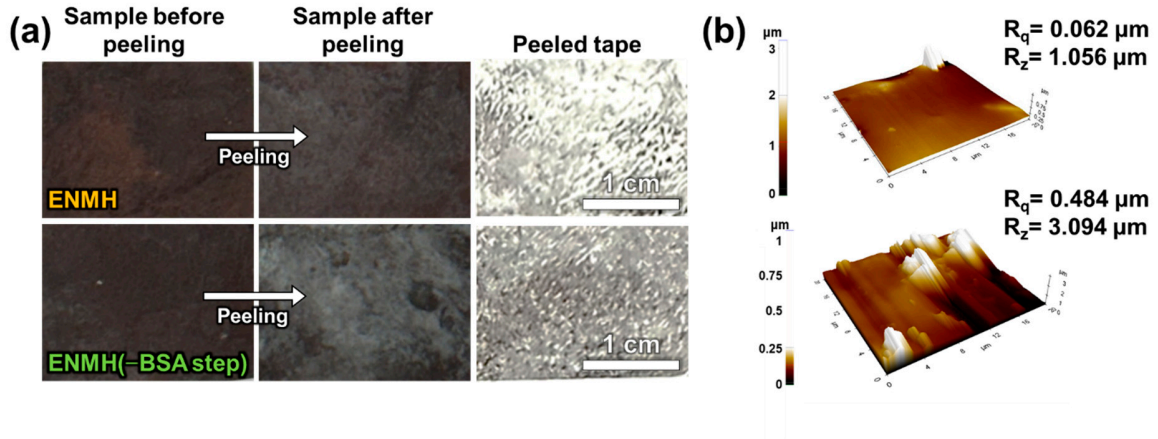


Figure S3. Photographic images of ENMH and ENMH(−BSA step), with surface conditions before and after the peel test. From left to right: Cu-coated nanofiber membrane before the peel test, after the peel test, and adhesive surface of the peeled tape. (b) 3D AFM images of the tape surface after a single peel test for both ENMH and ENMH(−BSA) samples (scan area: 20 × 20 μm^2).

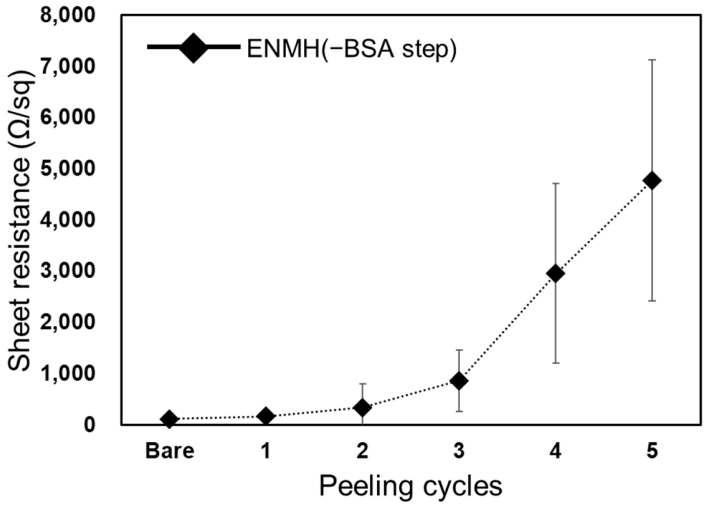


Figure S4. Variation in sheet resistance of ENMH(−BSA step) over repeated peel test cycles.

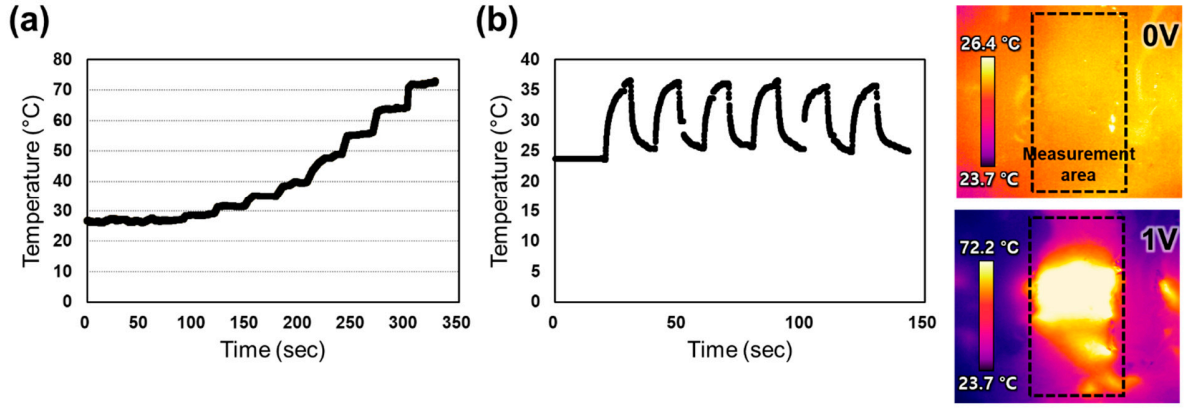


Figure S5. Thermal performance evaluation of the ENMH(−BSA step). (a) Stepwise voltage increase in 0.1 V increments every 30 s. (b) Short-term cyclic heating behavior under repeated ON/OFF switching of 0.6 V at 10 s intervals.

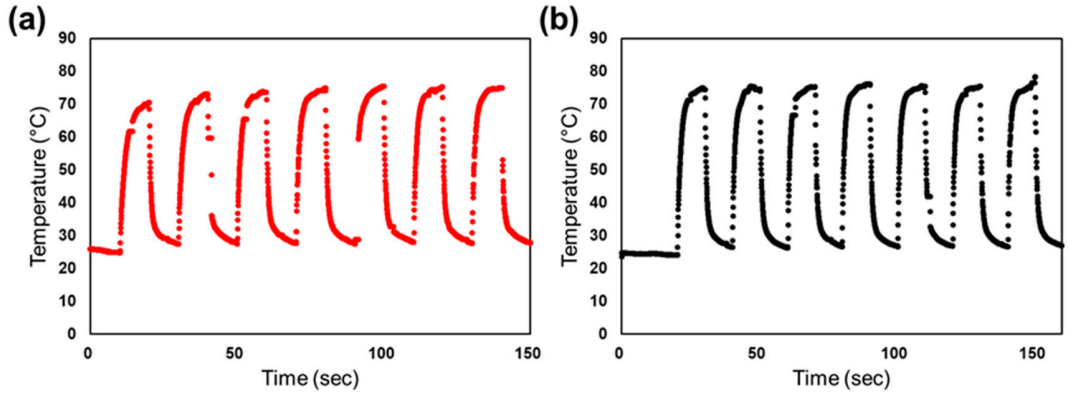


Figure S6. Environmental durability evaluation of the ENMH. (a) Temperature response of the ENMH under oxidative conditions (85 °C for 48 h) during stepwise voltage increments of 0.1 V every 30 s. (b) Temperature response to the same voltage increments after exposure to a humid environment (85% relative humidity at 25 °C).

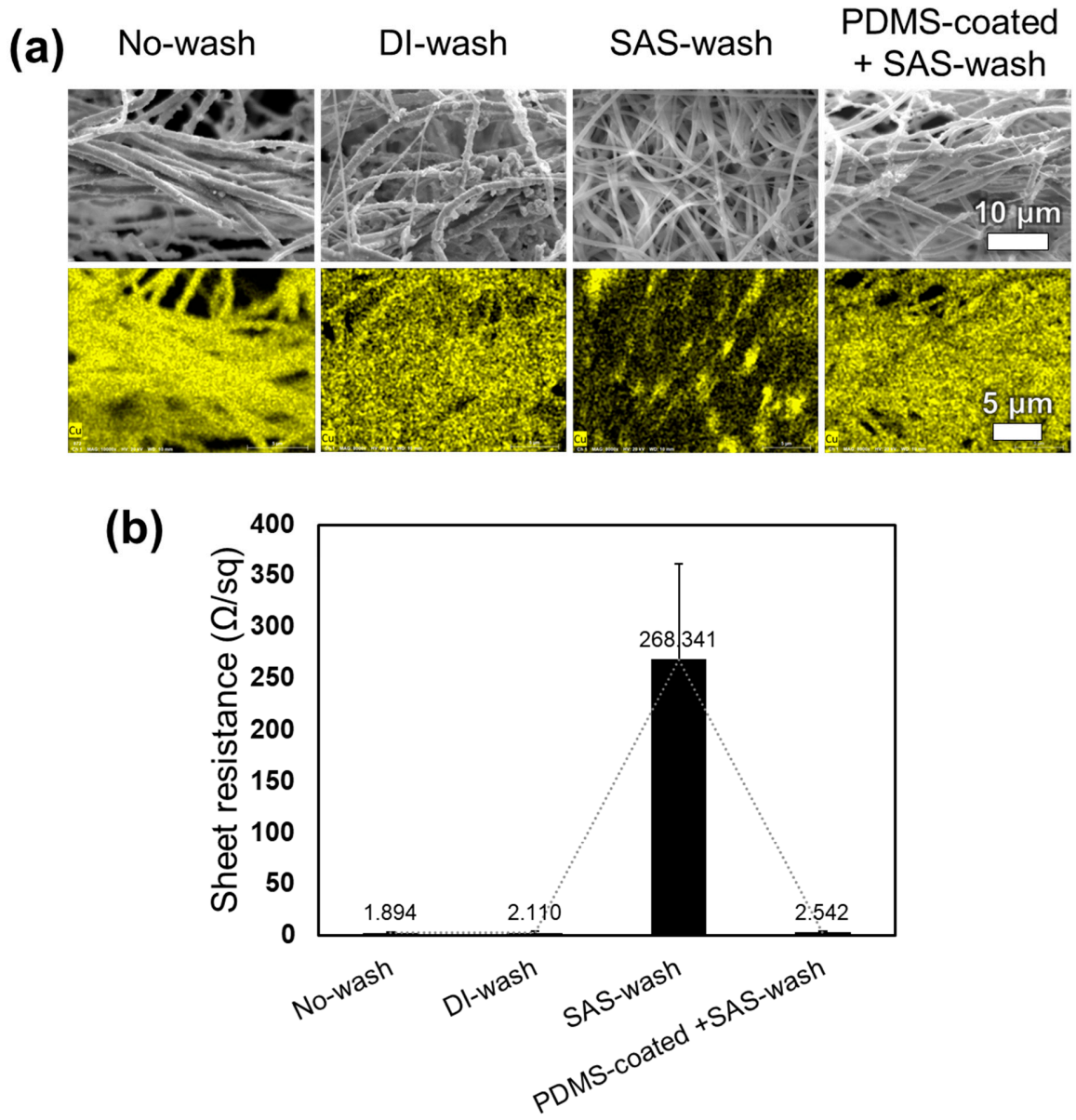


Figure S7. Evaluation of wash durability. (a) Surface SEM and EDS images of the ENMH after washing under different conditions. (b) Comparison of electrical conductivity corresponding to each washing condition.

No.	Electroactive Material	Type of Textile	Voltage (V)	Temperature (°C)	Electrical Properties	Refs.
1	Copper	PVDF-HFP nanofibers mat	1	124.1	1.894 Ω/sq	This work
2	$Ti_3C_2T_x$ MXene	Polyester Textile	4	79	1000 S/m	[55]
3	Ag@$Ni_xCo_{1-x}Se$ NWs/rGO/PDMS	Woven Kevlar fiber (WKF)	2.1	79	~10^3 Ω	[56]
4	Carbon nanotube	Cotton fabric	6	101	-	[57]
5	Carbon black/PU composite	Fabric	20	85	71 Ω/cm	[58]
6	AgNPs/CNT composite	Cotton fabric	5	120	0.8 Ω/sq	[59]
7	rGO/PEDOT:PSS	Cotton fabric	30	70	150 Ω/sq	[60]
8	Graphene/PVDF-HFP composite	Multilayer cotton-based fabric	30	85	-	[61]

Table S1. Comparison of the heating performance with recently reported textile-based wearable heaters.